Numerical Simulation of the Detailed Flow and Flame Propagation in a Homogeneous-Charge, Spark-Ignition Engine

K.Naitoh
NISSAN Motor Co., Ltd.
1 Natsushima-cho,
Yokosuka 237
Japan
K.Kuwahara
Institute of Space and Astronautical Science

ABSTRACT

Three-dimensional computations are performed to describe the details of the intake, compression, and expansion processes in a homogeneous-charge, spark-ignition engine. Emphasis is placed on the behavior of small vortices crushed by the piston during the compression process and the flame propagation influenced by these vortices. The Navier-Stokes equations are solved without using any explicit turbulence models. As to the chemical reaction, a one-step reaction model of octane, which obeys the Arrhenius Kinetics Law, is incorporated in the computations. An extended version of the MAC method is developed to simulate. A third-order upwind scheme is combined with this method. By extensive visualizations of the computed results, it is clearly shown that a large mushroom-shaped vortex, which is generated during the intake-stroke, breaks down into small-sized ones during the compression stroke. The numerical results also display that, after ignition sets in, the propagating flame is wrinkled with the curvatures over the grid size. It is qualitatively demonstrated that the propagation speed of this wrinkled flame is higher than that of the smooth flame which would be seen in the flow field when the intake and compression strokes are not taken into account.

INTRODUCTION

In the homogeneous-charge, spark-ignition engine, it has been documented that, near the end of the compression process, turbulence intensity increases in the combustion-chamber(1-3). It has been thought that a large mushroom-shaped vortex is generated during the intake-process, and this subsequently breaks down to a large number of small vortices toward the end of the compression process. This behavior is attributed to the fact that, as the process progresses, the effective area between the head and piston is reduced in comparison with the bore of the cylinder. This phenomenon is observed even for engines which do not have a squish area. The time-dependent flow and thermal structures are extremely complicated, and pertinent physics remains to be explored further.

In order to acquire an improved understanding of these important and complex flow fields, an efficient finite-differencing technique was developed to solve the governing Navier-Stokes equations and detailed three-dimensional numerical computational studies were performed (3-5). No explicit turbulence models were introduced.

In the present study, a simple engine with a curved intake port and a flat head is considered. The first phase of the computations is concerned with portraying the evolution of a large mushroom-shaped vortex which is generated in the intake-process. The break-up of this vortex into a large number of small vortices is numerically simulated in the compression process. The second phase of the computations will deal with the flow field when a one-step chemical reaction model of octane, which obeys the Arrhenius Kinetics Law, is incorporated in the numerical computations. It will be qualitatively seen that the flame is wrinkled by an influence of the small vortices, though the subgrid turbulence model and modelling on flame are not taken into account. The propagation speed of this wrinkled flame is higher than that of the smooth flame which would be seen in the flow field when the intake and compression strokes are absent.

MATHEMATICAL FORMULATION AND NUMERICAL MODEL

The Basic Equations

The following governing equations are expressed in non-conservative form :

$$\frac{D\rho}{Dt} + \rho\, u_{i,i} = 0 \qquad (1)$$

$$\frac{Du_i}{Dt} + \frac{1}{\rho} p_{,i} = \frac{1}{\rho} \sigma_{ij,j} \quad (2)$$

$$\frac{Dh}{Dt} = \frac{1}{\rho}\frac{Dp}{Dt} - \frac{1}{\rho} q_{i,i} + \frac{\dot{Q}}{\rho} + \frac{1}{\rho}\sigma_{ij}(u_{i,j}) \quad (3)$$

$$\frac{DY_m}{Dt} = \dot{Y}_m - \frac{1}{\rho}[\rho J_{mi}]_{,i} \quad (4)$$

$$p = \rho RT \quad (5)$$

The dependences of viscosity is modeled by the Sutherland laws, and the Prandtl number is taken to be 0.7. The Schmidt number is set to be 1.0 in the entire calculations. The constant-pressure specific heat Cp for air is simply approximated by the linear function of temperature in the practical temperature range between 300 K and 3000 K (6):

$$Cp = C_0 + \frac{1}{2} C_1 T \quad (6)$$

In addition, the gas constant is taken to be the value for air.

The numerical solution technique to tackle the above set of equations is an extended version (3-5) of a well-known numerical algorithm (7-9). The specifics of the numerical methods are summarized in the Appendix. No explicit turbulence models are used in this numerical computation scheme.

Chemical Reaction and Ignition

In this investigation, the one-step chemical reaction is considered only for octane. The progress rate $\dot{\omega}$ is modeled by the well-known formula (10):

$$\dot{\omega} = A\exp(-E/RT)\,[\rho_f/W_f]^{a_f}\,[\rho_o/W_o]^{a_o} \quad (7)$$

in which $A=4.6\times10^{11}$ $(mol/cm^3)^{1-a_f-a_o}.sec.^{-1}$, $E=30.0$ kcal/mole, $a_f=0.25$, $a_o=1.5$.

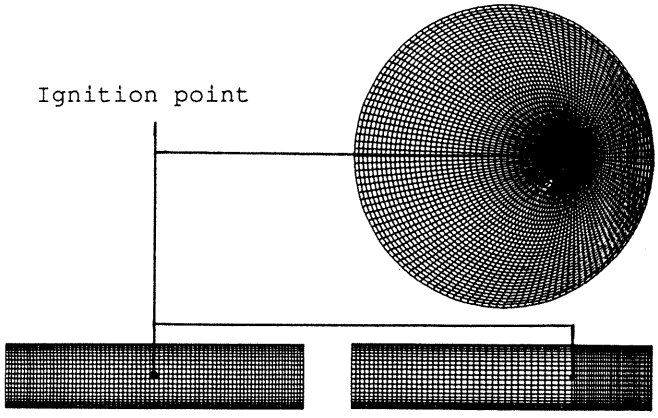

Fig. 1 The grid system (20x40x128points)

In order to deal with the ignition, a constant temperature of 2500 K is prescribed at the ignition point during two degrees after 330degATDC. The ignition point is depicted in Fig. 1.

Initial and Boundary Conditions

First of all, the potential flow is obtained, when the crank angle reaches 100 degATDC during the intake process. After the timing, the subsequent flow in the intake process is calculated by resorting to the full governing equations under the assumption of the incompressible flow approximation. The flow field obtained at the end of the intake process is used as the initial conditions for the computations in this study.

As to the boundary conditions at the walls, non-slip conditions are specified for the velocity field. Iso-thermal wall conditions are adopted in this study. For the pressure field, Neumann-type conditions are utilized (11).

Grids and Computational Particulars

The number of computational time steps is 1080 per engine cycle. The number of grid points employed is 20x40x128, and the grid size is the magnitude of about 1 cu mm at each point. The grid system is shown in Fig. 1. The computational particulars are listed in Table I.

COMPUTATIONAL RESULTS AND DISCUSSION

Flow in the Compression Process

Figure 2 displays exemplary evolutions of the computed flow fields during the intake and compression processes for CASE II. Near the end of the intake process [see Fig. 2(a)], the cylinder area is large and the formation of a large mushroom-shaped vortex is clearly seen. Toward the end of the compression stroke [see Fig.2(b-d)], the chamber height has decreased well below

Table I The computational particulars

	CASE I	CASE II
Initial flow	when the flows in the intake and compression processes are neglected	when the flows in the intake and compression processes are present
Engine speed	1400 /min	
Charging efficiency	30 %	
Equivalence ratio	1.0	
Wall temperature	400K	
Compression ratio	8.0	
Bore	85 mm	
Stroke	86 mm	
Ignition timing	30 deg BTDC	

the size of the bore of the cylinder. The resulting vortices are of the scales smaller than the chamber height. As is apparent in Fig. 2, the squeezing action of the piston is responsible for the generation of these small-scale vortices near the end of the compression stroke.

Flame Propagation

The computational results for the temperature field are shown in Fig. 3 for CASE I. The iso-thermal surface of 1500K is presented. As stated earlier, this case refers to the situation in which the initial flows due to the intake and compression strokes are not taken into account in the computations. Obviously, the smooth laminar flame is in evidence. And also, in the side view, the tulip-shaped flame is seen.

Figure 4 shows the temparature contours in CASE II. As is evident in Fig. 4, the shape of the flame is wrinkled as the ignition process progresses. This is caused primarily by the small vortices that have been generated during the compression process. At 380 degATDC [in top view of Fig. 4(d)], it is worth pointing out that a region of unburned gas exists near the cylinder wall in upper-right. This reflects the fact that the flame propagation is appreciably influenced by the large-scale swirling motion due to the asymmetric configuration of the intake-port. It is stressed that the computational conditions are identical, except for the existence of the initial flow, for both Fig. 3 and 4. However, the propagation speeds of the flame demonstrate differences. It is faster in CASE Il than in CASE I; one principal explanation lies in the fact that the surface of the flame in CASE lI is larger than in CASE I due to the distorted and wrinkled shape of the flame front.

In order to ascertain the above-mentioned qualitative differences between CASE I and CASE II, the computed results have been further processed to extract more quantitative information. One physically meaningful variable is the total volume [TV] of the region of combustion. In the present study, this is somewhat arbitrarily defined as the volume for which the temperature lies in the range between 1000K and 2000K. Figure 5 displays the time-history of TV for the two cases. It is clear that TV for CASE II is bigger than that of CASE I. This observation is further corroborated by inspecting similar plots for pressure in Fig. 6. The results are supportive of the earlier contention that the initial flow in the cylinder is responsible for the increases in the flame speed. The increase of the flame speed obtained by this simulation model is due to turbulence and flame fructuation which have magnitude over grid size. Subgrid turbulence model and modelling on the flame are needed to estimate the flame speed quantitatively. It is because the kolmogolov scale and the flame thickness are about 0.1mm in this condition.

Figure 7 is a representative plot exhibiting the qualitative shape of the flame front at the crank angle of 370degATDC. The flame front here is illustrated by drawing five contour lines of temperature, ranging from 1000K to 2000K in a cross section. In the present plots, the temperature gradient in the burning region is close to 1000K over a distance of one millimeter. Also shown in Fig. 7 are the streamlines projected on the center surface betwen the head and piston. The existence of vortices and the expanding flow patterns, which are due to the heat release of the chemical reaction, near the flame front are illustrated in this figure.

CONCLUDING REMARK

In the intake-process, a large mushroom-shaped vortex is generated near the intake valve. It is calculated that this vortex is broken into smaller vortices during the compression stroke without using any turbulence model. This is mainly caused by the shrinking chamber height. After ignition, an increase of the flame propagation speed by the vortices is calculated, though the above-mentioned results do not consider the effect of subgrid turbulence to the flame speed.

NOMENCLATURE

a	exponent which specify the order of reaction
A	pre-exponential in the Arrhenius Kinetics Law
$C_p \left(\equiv \sum_{m=1}^{m_{max}} \sum_{\alpha=0}^{\alpha_{max}} \frac{Y_m}{(\alpha+1)} C_{\alpha m} T^{\alpha}\right)$	constant-pressure specific heat
$C_p' \left(\equiv \sum_{m=1}^{m_{max}} \sum_{\alpha=0}^{\alpha_{max}} Y_m C_{\alpha m} T^{\alpha}\right)$	$C_p' = d[C_pT]/dT$
Dm	molecular diffusivity of species m
$D/Dt = \partial/\partial t + u_i \partial/\partial x_i$	substantial derivative
E	activation energy
$h \left(\equiv Cp\ T\right)$	entalphy
$J_{m\,i} \left(\equiv - D_m Y_{m,i}\right)$	molecular diffusion flux of the m th species
k	thermal conductivity
p	pressure
$\dot{Q}$	heat release by chemical reaction
$q_i \left(\equiv - kT_{,i}\right)$	heat flux
R	gas constant
T	temperature
u_i	velocity vector
V	the entire volume of the cylinder

W	molecular weight
Ym	mass fluction of species m
μ	viscosity coefficient
$\dot{\omega}$	rate of progress by chemical reaction
ρ	density
$\sigma_{ij,j}$ $(\equiv\mu u_{i,jj} + 1/3\ \mu(u_{j,j})_{,i})$	viscous stress tensor

Subscripts

f	fuel
m	species $(O_2, H_2O, C_8H_{18}, CO_2, N_2)$
o	oxygen

ACKNOWLEDGEMENT

The authors express sincere thanks to Prof. M. Hyun of Korea Advanced Institute of Science and Technology for his advices and to Dr. Shirayama of the Institute of Computational Fluid Dynamics for his assistance in generating the graphic outputs of the results.

REFERENCES

1. A.D.Gosman, Y.Y.Tsui,and C.Vafidis : "Flow in a Model Engine with a Shrouded Valve", SAE paper 850498, 1985.
2. D.Foster and P.Witze : "Two-Component Laser Velocimeter Measurements in a Spark Ignition Engine", Combust. Sci. and Tech.: Vol. 59, p.85, 1988.
3. K.Naitoh, Y.Takagi, K.Kuwahara, E. Krause, and K.Ishii : "Three Dimensional Computation of Transition to Turbulence in a reciprocating Engine", AIAA paper 89-1886, 1989.
4.K.Naitoh, H.Fujii, Y.Takagi, andK. Kuwahara : "Numerical Simulation of the Detailed Flow in Engine Ports and Cylinders", SAE paper 900256, 1990.
5. K.Naitoh, E.Krause, and K.Kuwahara : to be published in the 12th International Conference on the Numerical Method of the Fluid Dynamics, 1990.
6. JANAF Thermodynamic Tables, U. S. Government Printing Office, Washington, D. C., 1971.
7. T.Kawamura and K.Kuwahara : "Direct Simulation of a Turbulent Inner Flow by Finite-Difference Method", AIAA paper 85-0376, 1985.
8. T.Kawamura and K.Kuwahara : "Computation of High Reynolds number Flow around a Circular Cylinder with Surface Roughness", AIAA paper 84-0340, 1984.
9. K.Kuwahara : "Computation of Thermal Convection with Large Temperature Difference", Proceeding of the Fourth International Conference on Applied Numerical Modeling, p. 565, 1984.
10. C.K.Westbook and F.L.Dryer : "Simplified Reaction Mechanisms for the Oxidation of Hydrocarbon Fuels in Flames", Combust. Sci. and Tech., Vol.27, p.31, 1981.

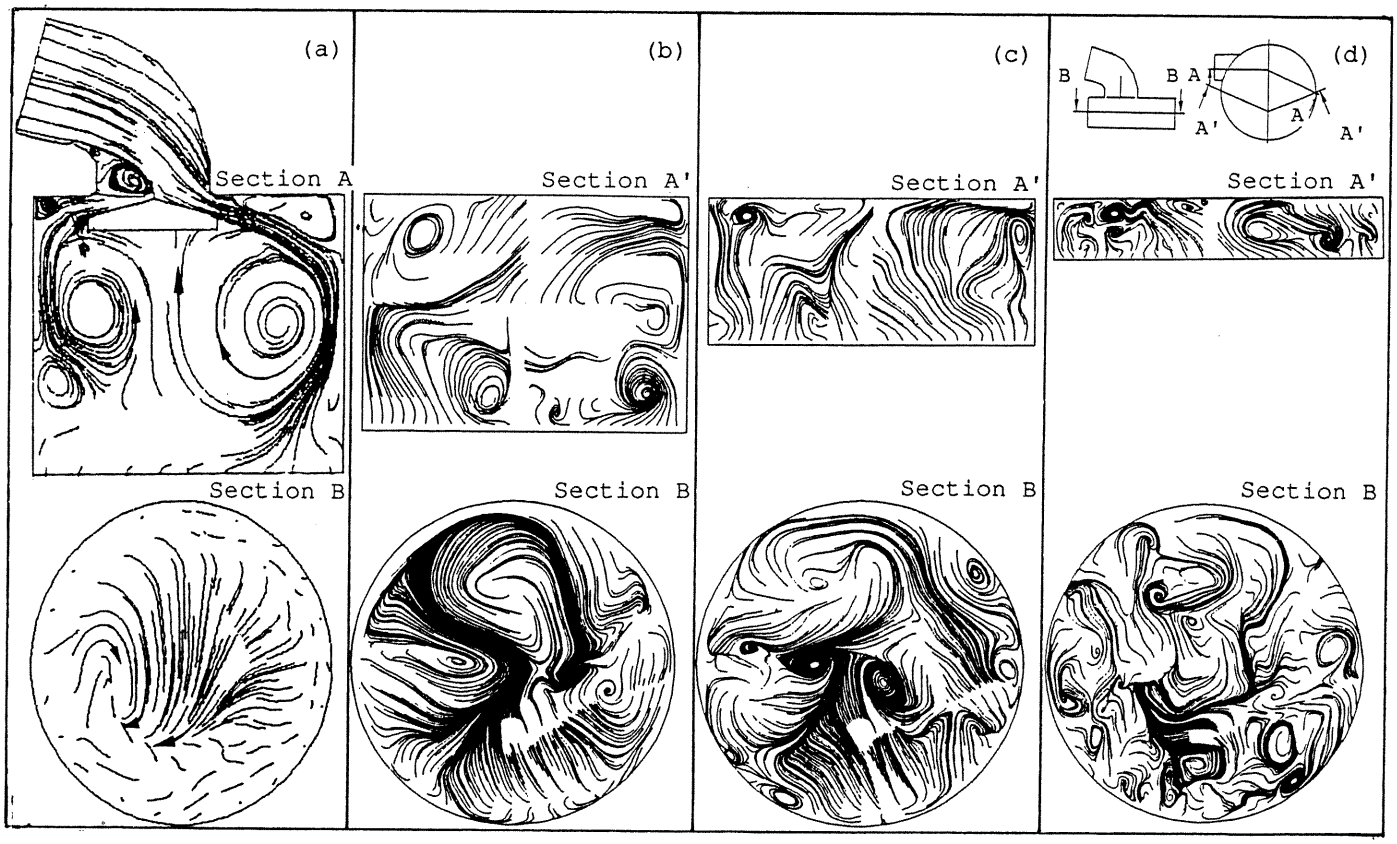

Fig. 2 The streamlines projected on some cross sections near the end of the intake process
(a) Crank Angle=160degATDC (c) Crank Angle=270degATDC
(b) Crank Angle=240degATDC (d) Crank Angle=320degATDC

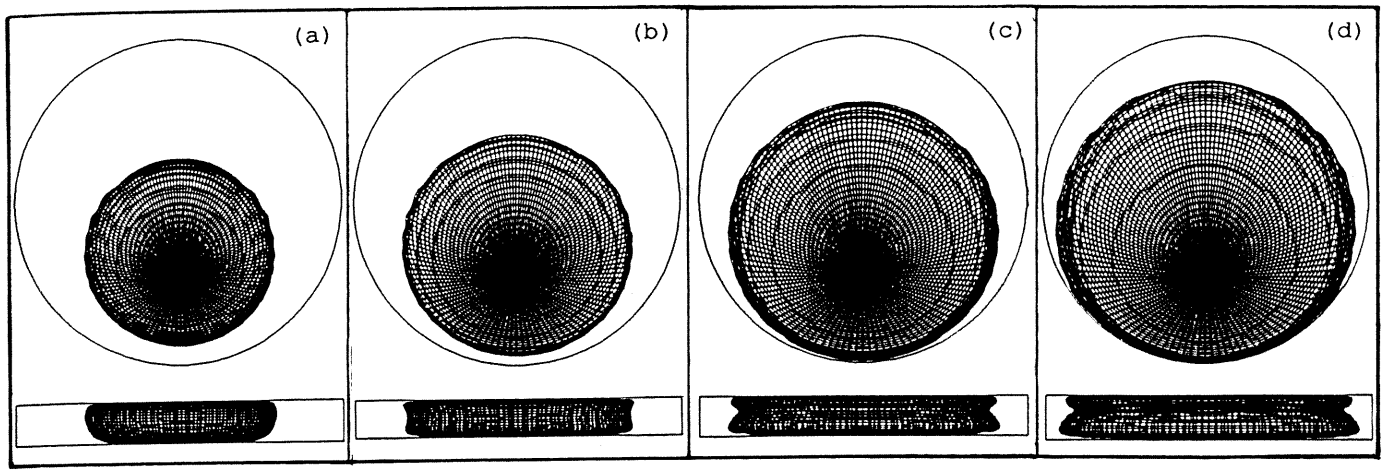

Fig. 3 The iso-thermal surface of 1500K after ignition (CASE I)
(a) Crank Angle=350degATDC (c) Crank Angle=370degATDC
(b) Crank Angle=360degATDC (d) Crank Angle=380degATDC

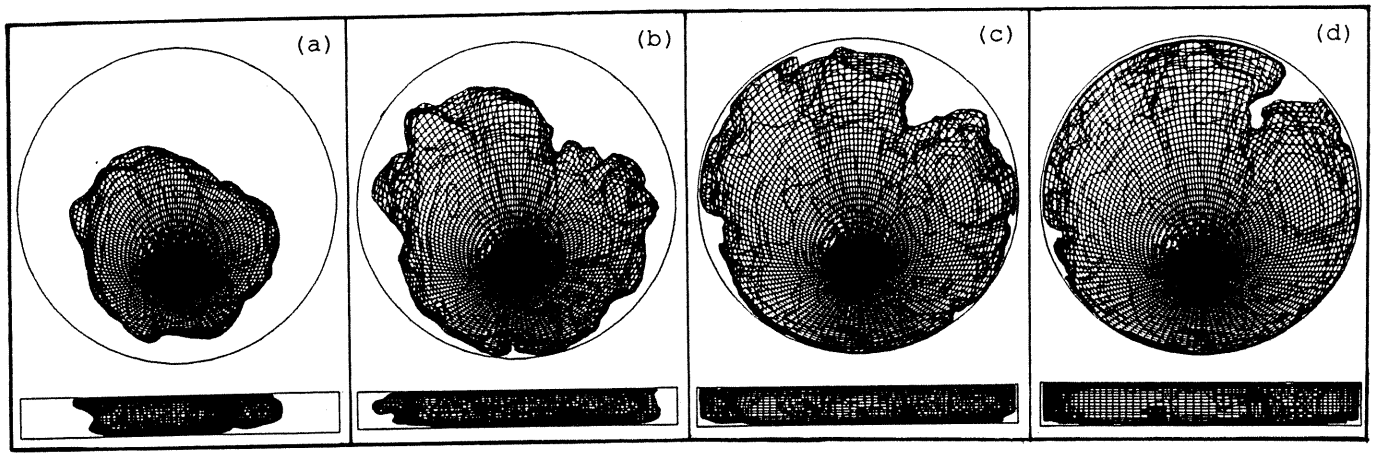

Fig. 4 The iso-thermal surface of 1500K after ignition (CASE II)
(a) Crank Angle=350degATDC (c) Crank Angle=370degATDC
(b) Crank Angle=360degATDC (d) Crank Angle=380degATDC

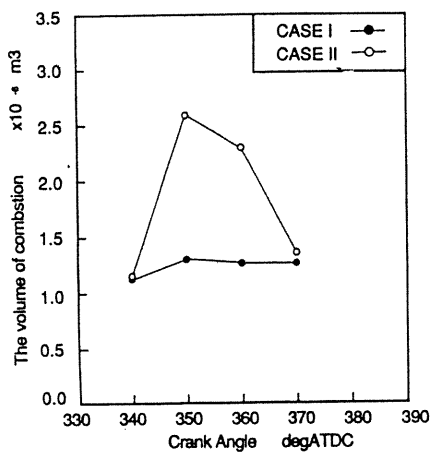

Fig. 5 The time history of the combusting volume

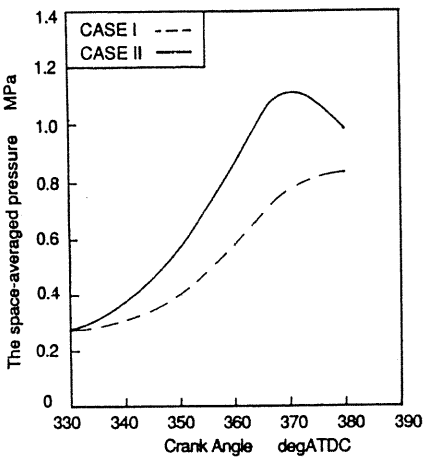

Fig. 6 The time history of the space-averaged pressure

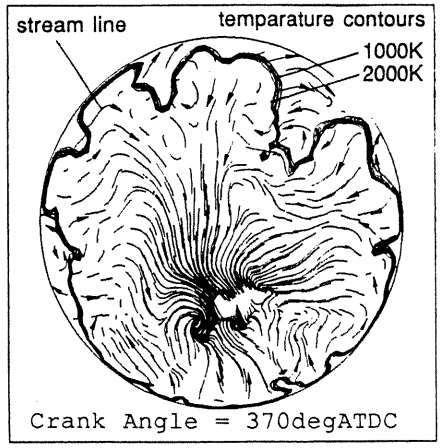

Fig. 7 The temparature contours and streamlines projected on a cross section

11. K.Naitoh, Y.Yoshikawa, H.Fujii, and Y.Takagi : "A Higher-Order Accurate Computation of Three Dimensional Flow in the Intake-Stroke of a Reciprocating Engine", Vol. 55 No. 515, p.1868. J. S. M. E., 1989.
12. A.Majda and J.Sethian : "The Derivation and Numerical Solution of the Equations for Zero Mach Number Combustion", Combst. Sci. and Tech., Vol. 42, p.185, 1984.
13. F.H.Harlow and J.E.Welch : "Numerical Calculation of Time-dependant Viscous Incompressible Flow of Fluid with Free Surface", Physics of Fluids, Vol.8, No.12, p2182 , 1965.

APPENDIX: the Basic Equations and the Numerical Method

The three scalar variables are split into two parts, as shown below:

$$p = p_1(t) + p_2(t,x), \qquad \int_v p_2(t,x)dV = 0 \tag{A.1}$$

$$T = T_1(t) + T_2(t,x), \qquad \int_v T_2(t,x)dV = 0 \tag{A.2}$$

$$\rho = \rho_1(t) + \rho_2(t,x), \qquad \int_v \rho_2(t,x)dV = 0 \tag{A.3}$$

In the cylinder of engines, even in the case with combustion, the local Mach number would be under 0.3 even at high engine-speed. In such cases, the following approximated state of equation can be used instead of Eq. (5) (12).

$$\frac{dp_1}{dt} = \frac{D\rho}{Dt}RT + \rho R\frac{DT}{Dt} \tag{A.4}$$

Also adopting this assumption into Eq. (3), the following equaiton is obtained.

$$\frac{DT}{Dt} = \frac{1}{\rho C_p'}\left[\left(\frac{dp_1}{dt}\right) + \sigma_{ij}u_{i,j} + \dot{Q} - q_{i,i}\right] \tag{A.5}$$

For computation, Eq. (1) are transformed using Eqs. (A.4) and (A.5) as follows.

$$u_{i,i} = \frac{1}{\rho C_p'T}\left[\sigma_{ij}u_{i,j} + \dot{Q} - q_{i,i}\right] + \frac{1}{p}\frac{dp_1}{dt}\left[\frac{R}{C_p'} - 1\right] \tag{A.6}$$

Taking the divergence of Eq.(2),

$$\left[\frac{1}{\rho}p_{2,i}\right]_{,i} = -\frac{\partial u_{i,i}}{\partial t} - [u_i u_{j,i}]_{,i} + \left[\frac{1}{\rho}\sigma_{ij,j}\right]_{,i} \tag{A.7}$$

Computations are performed by the following four step algorithm.

[1st step]

$$\frac{DY_m^{n+1}}{Dt} = \dot{Y}_m^n - \frac{1}{\rho}[\rho J_{m\,i,i}]^{n+1} \tag{A.8}$$

[2nd step]

$$\frac{DT_2^{n+1}}{Dt} = -\frac{dT_1}{dt}^{n+1} + \frac{1}{(\rho C_p')^n}\left[\left(\frac{dp_1}{dt}\right)^{n+1} + \dot{Q}^n - q_{i,i}^{n+1}\right] \tag{A.9}$$

$$\left[\frac{dp_1}{dt}\right]^{n+1}\left[\int\left(1-\frac{R}{C_p'}\right)dV\right]^n + p_1{}^n\left[\frac{dV_{all}}{dt}\right]^{n+1} = \left[\int\frac{R}{C_p'}(-q_{i,i}+\sigma_{ij}u_{i,j}+\dot{Q})\,dV\right]^n \tag{A.10}$$

$$\left[\frac{1}{\rho_1}\frac{d}{dt}\rho_1\right]^{n+1} = \left[\frac{1}{V_{all}}\frac{d}{dt}V_{all}\right]^{n+1} \tag{A.11}$$

$$\int \rho_2^{n+1}(t,x)dV = 0 \tag{A.12}$$

$$\int T_2^{n+1}(t,x)dV = 0 \tag{A.13}$$

$$p_1{}^{n+1} = \rho^{n+1}RT^{n+1} \tag{A.14}$$

[3rd step]

$$\left[\frac{1}{\rho^{n+1}}p_{2,i}{}^{n+1}\right]_{,i} = -\frac{1}{\delta t}\left[\frac{1}{\rho C_p'T}(\dot{Q} - q_{i,i}) + \frac{1}{p}\frac{dp_1}{dt}\left(\frac{R}{C_p'} - 1\right)\right]^{n+1} + \frac{1}{\delta t}u_{i,i}{}^n - [u_i u_{j,i}]_{,i}{}^n \tag{A.15}$$

$$\int p_2^{n+1}(t,x)dV = 0 \tag{A.16}$$

[4th step]

$$\frac{Du_i^{n+1}}{Dt} + \frac{1}{\rho^{n+1}}p_{,i}^{n+1} = \frac{1}{\rho^{n+1}}\sigma_{ij,j}^{n+1} \tag{A.17}$$

Equations (A.10) and (A.11) are obtained by integrating the mass and energy conservation laws spatially. The convective terms in Eqs. (A.8), (A.9) and (A.17) are finite-differenced by the third-order upwind scheme which is useful to the high Reynolds number flow (7-8). The other terms are estimated by the second-order central differencing. In time, the Euler bachward scheme is employed.

Numerical algorthm is based on the MAC method basically (13). As the values at the time step n are given, first Y_m is computed at the next time step by Eq. (A.8). Because the volume Vall are given, p1(t), T1(t), $\rho_2(t,x)$ and T2(t,x) are computed and the chemical reaction is calculated. And the Poisson equation for spatial variations of pressure is solved . Using these new values, the velosity vector is solved finally. Details of the numerical algorithm are described in references (3-5).